arXiv:astro-ph/0502351v1 17 Feb 2005

The High-Energy Polarization-Limiting Radius of Neutron Star Magnetospheres II – Magnetized Hydrogen Atmospheres

Jeremy S. Heyl[⋆,1], Don Lloyd[⋆], and Nir J. Shaviv[†]

[⋆] *Harvard College Observatory, MS-51, 60 Garden Street, Cambridge, Massachusetts 02138, United States*

[†] *Racah Inst. of Physics, Hebrew University of Jerusalem, Jerusalem 91904, Israel*

ABSTRACT

In the presence of strong magnetic fields, the vacuum becomes a birefringent medium. We show that this QED effect couples the direction of the polarization of photons leaving the NS surface, to the direction of the magnetic field along the ray's path. We analyze the consequences that this effect has on aligning the polarization vectors to generate large net polarizations, while considering thermal radiation originating from a thermal hydrogen atmosphere. Counter to previous predictions, we show that the thermal radiation should be highly polarized even in the optical. When detected, this polarization will be the first demonstration of vacuum birefringence. It could be used as a tool to prove the high magnetic field nature of AXPs and it could also be used to constrain physical NS parameters, such as R/M, to which the net polarization is sensitive.

1. Introduction

Neutron stars provide an exciting laboratory to understand extreme realms of physics. Processes in their interiors probe nuclear theory in uncharted regimes, and not only is the surrounding spacetime strongly curved but also it is often pervaded by a strong magnetic field. As radiation from the surface of the star traverses this region, both the curvature of the spacetime and the strong magnetic field leave traces. It is possible to unravel these two processes to verify that the magnetic field of the star does indeed interact with the outgoing radiation (a prediction of quantumelectrodynamics) and that the spacetime exterior to the star curves the trajectories of the rays.

In several earlier papers (Paper I: Heyl et al. 2003; Heyl & Shaviv 2002; Shannon & Heyl 2004) we have examined how the magnetosphere of a neutron star affects the propagation of polarized radiation from the surface of the star. In all of these papers we assumed a very simple model for the

[1]Chandra Postdoctoral Fellow, Current Address: Department of Physics and Astronomy, University of British Columbia 6224 Agricultural Road, Vancouver, British Columbia, Canada, V6T 1Z1

atmospheric emission: the emission is fully polarized at all frequencies. In this paper we combine a realistic treatment of the radiative transfer of the magnetosphere as in the earlier works with an accurate calculation of the radiative transfer within in the highly magnetized hydrogen atmosphere of the neutron star (Lloyd 2003). Although several authors have recently focussed on the emission properties of neutron star atmospheres (for example Lai & Ho 2003b; Özel 2001; Zane et al. 2001), these techniques have focussed on the case where the magnetic field is perpendicular to the surface of the star. The models used here consider the important, general (and more difficult to calculate) case where the magnetic points in a arbitrary direction. Furthermore, we have used the envelope models of Heyl & Hernquist (1998a) and Heyl & Hernquist (2001) to determine the flux at each point on the star.

Although these atmosphere models treat general magnetic geometry, they lack several features included in other models. These effects such as vacuum polarization in the atmosphere itself (Lai & Ho 2003a), the proton-cyclotron resonance (Zane et al. 2001; Özel 2003) and partial ionization Ho et al. (2003) may be important to understand some details of the emission at certain magnetic field strengths. However, the general properties of the polarization spectral energy distribution of magnetized neutron-star atmospheres is unlikely to depend strongly on these processes.

Although such mangetized hydrogen atmospheres provide a good explanation of the data from some neutron stars (Perna et al. 2001a,b), some of the more well studied objects such as RX J1856.5-3754 remain inscrutable (Turolla et al. 2004). Chang et al. (2004) has argued that the hydrogen atmosphere of a magnetar ($B \gtrsim 10^{14}$ G) is consumed by diffusive nuclear burning within a few thousand years, leaving a surface layer of helium. On the other hand, the hydrogen layer reamins on the surface of more weakly magnetized neutron stars for up to one hundred times longer (Chang & Bildsten 2004). Because our focus here is on both magnetars and more weakly magnetized young neutron stars, we will assume that hydrogen comprises the atmospheres of these objects. It is likely that a fully ionized helium atmosphere exhibits grossly similar emission properties.

In the following sections we describe the calculations in modest detail (§ 2) – the reader is encouraged to look at the authors' earlier works for further details (e.g. Heyl et al. 2003; Lloyd 2003). A detailed exposition of the results of these calculations (§ 3) follows. This includes a comparison with earlier results (§ 3.3). In § 4 we place

our results in the greater context.

2. Calculations

Calculating the emergent polarized spectra from neutron stars requires several ingredients. As we argued in Paper I, the general relativistic corrections to the field geometry may be neglected, so we assume that the field geometry is a centered dipole. We use the results of Heyl & Hernquist (1998, 2001) to determine the emergent energy flux over the surface of the star. We use the results of Lloyd et al. (2003) and Lloyd (2003) to calculate the emergent photon spectrum at a grid of points

on the surface. Finally, we construct the image of the neutron star surface by tracing rays from the surface of the neutron star to the detector. The final spectrum is obtained by interpolating the polarized intensities from the grid of atmosphere models and summing over the calculated image. In the next subsections, we will outline each step of this process in further detail.

2.1. Atmospheric Spectra

We assume that the total flux at each point (ϕ, β) of the NS surface is proportional to

$$F \propto B^{0.4} \cos^2 \psi, \tag{1}$$

where ψ is the angle between the local normal and the direction of the magnetic field and B is the magnitude of the field. This was shown to result from the effect that the magnetic field has on heat transfer throught he NS crust (Heyl & Hernquist 1998a, 2001). We use atmosphere models calculated at $B = 10^{12}$ G and 10^{14} G. For the stronger field, the atmosphere calculation converges much more quickly for higher fluxes, so we use a model with $T_{\rm p,eff} = 10^{6.5}$ K. At 10^{12} G we use $T_{\rm p,eff} = 10^{6.5}$ K for comparison with the 10^{14} G results and $T_{\rm p,eff} = 10^{6}$ K for comparison with the results of Pavlov & Zavlin (2000). The models of Pavlov & Zavlin (2000) did not account for the temperature distribution across the surface of the star, so we also calculated a model with $T_{\rm eff} = 10^{6}$ K over the entire star.

Although some subtle details of the emergent spectra depend on the value of the surface gravity, we are only concerned with the gross polarization of the emergent radiation; therefore, we adopt a canonical value of $g_s = 2.4 \times 10^{14}$ cm s^{-2}. This simplification reduces the number of atmosphere calculations by a factor of three.

The polarized spectrum is derived numerically from a self-consistent solution to the equations radiative transfer for a stationary, plane-parallel atmosphere in radiative equilibrium. We adopt the simplifying assumption that the atmospheric plasma is pure hydrogen in the limit of complete ionization, for which the opacity sources are inverse bremsstrahlung, Thomson scattering, and resonant scattering by protons. The magnetic field is assumed to be vertically uniform. The atmospheric model is obtained by the method of complete linearization (Mihalas 1978), starting from a power-law prescription for the conductivity of the plasma as a trial solution (Heyl & Hernquist 1998b). Convergence is achieved ($\delta T/T < 10^{-3}$) typically within 10-20 iterations; flux is conserved to about 10^{-4} at all depths.

Radiative transport proceeds in two coupled normal modes of polarization, uniquely defined for propagation angle θ_B with respect to the direction of $\vec{B}$. The magnetic field induces a strong angular dependence in the plasma opacity, and suppresses the opacity by a factor $(E_\gamma/E_{cyc}$ in one mode of propagation (Ventura 1979). Consequently, the emergent flux is dominated by the "extraordinary mode" which sees a more transparant medium over a broad range of θ_B. To the best of our knowledge, these models are the first models to employ complete linearization and to

consider neutron-star atmospheres where the magnetic field is slanted with respect to the normal.

2.2. Integrated Spectrum

Once a polarization "image" is calculated (see Paper I for details), the net polarization seen by an observer is found by integrating the intensity contributed by each of the normal modes of the atmosphere to each of the observed Stokes's parameters, adapting the results of Perna et al. (2001b), we have

$$S_{i,\nu} = \frac{1}{4\pi D^2(1+z)^3}\int_0^{b\max} bdb\int_0^{2\pi} d\beta \times \left[|\langle S_i|U|X\rangle|^2 I_{X,\nu(1+z)}(\phi,\beta;\delta,\upsilon) + |\langle S_i|U|O\rangle|^2 I_{O,\nu(1+z)}(\phi,\beta;\delta,\upsilon)\right] \quad (2)$$

in units of erg cm^{-2} s^{-1} keV^{-1}. Here $x = \sin\delta = b/R_\infty$ ($R_\infty = R(1+z)$ and δ is the apparent zenith angle of the observer from a point on the surface), $b_{\max} = R_\infty$ for $R > 3M$ and $b_{\max} = 3\sqrt{3}M$ for $R \leq 3M$. The gravitational redshift at the surface is given by $1+z = (1-2M/R)^{-1/2}$. $I_{O,\nu}$ and $I_{X,\nu}$ are the intenisty per unit frequency per unit solid angle emitted at the surface, in the ordinary and extraordinary modes respectively. ϕ, β and δ are defined in § 2.2 of Paper I. υ is the azimuth of th line of the sight from the surface.

The general relativistic effects of light deflection are taken into account through the ray-tracing function, $\phi(x)$ (Page 1995, and §2.2 of Paper I)). As previously mentioned, if $S_1/S_0 = 1$ is taken to denote light fully polarized perpendicular to the projection of the direction of the magnetic dipole moment, symmetry dictates that $S_2 = S_3 = 0$. The operator U accounts for the evolution of the polarization as the photon travels from the surface which Paper I discusses in detail.

3. Results

By combining the detail calculations of the radiative transfer through atmosphere with ray tracing through the magnetosphere including the evolution of the polarization, we obtain spectral energy distrubtions like those depicted in Fig. 1. A comparision of the total emergent flux in two magnetic fields shows that the more weakly magnetized atmosphere has a bluer spectrum; Lloyd et al. (2003) have noted this effect. In more detail, if we examine the results neglecting vacuum polarization (light curves), the emission from the more weakly magnetized atmosphere is also less polarized. The most important trend, which we shall explore in further detail, is apparent from comparing the light curves with the dark curves which include the effects of vacuum polarization in the magnetosphere. In both cases, the inclusion of vacuum polarization increases the polarized flux from $\sim 10\%$ to nearly 100%.

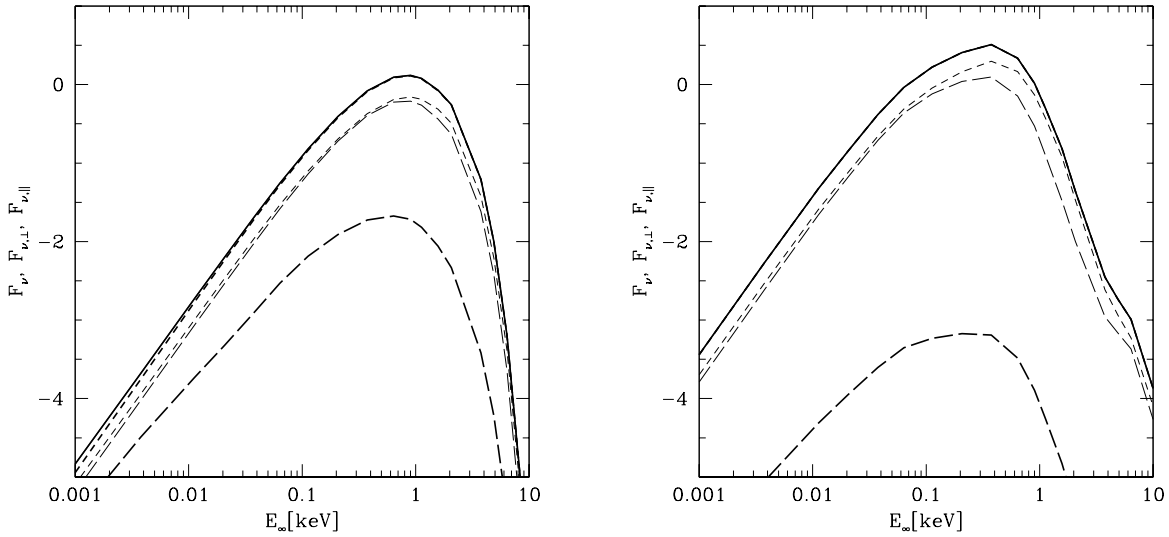

Fig. 1.— The total emergent flux from the visible surface of the star. The magnetic pole makes an angle of 60° with the line of sight. The radius of the star is 12 km and its mass is 1.4 $M_\odot$. The effective temperature at the magnetic pole is $10^{6.5}$ K. The left panel is for a magnetic moment of $\mu = 10^{30}$ G cm^3 and the right panel is for $\mu = 10^{32}$ G cm^3, corresponding to surface fields of $\sim 10^{12}$ G and $\sim 10^{14}$ G respectively. The solid curve traces the total flux. The short dashed curve traces the flux polarized perpendicular to the projection of the magnetic moment in the plane of the sky. The long-dashed curve traces the flux polarized parallel to the projected magnetic moment. The heavy curves trace the results including vacuum polarization and the light curves neglect it.

3.1. Dependence on Stellar Radius

Fig. 2 shows the extent of polarization as a function of energy and radius for 10^{12} G and 10^{14} G neutron stars. The observed net polarization depends strongly on both the strength of the magnetic dipole moment and the radius of the star. We find that smaller stars exhibit higher polarized fractions – this is the opposite of the Pavlov & Zavlin (2000) result. Although gravitational lensing is more important for the more compact stars and we *do* see a larger fraction of the stellar surface, the observed polarization direction reflects the direction of the magnetic field at the polarization-limiting radius *not* at the surface. The size of $r_{\rm pl}$ (*c.f.* eq. 16 of Paper I) is independent of the radius R of the star. Meanwhile as R decreases the solid angle subtended at $r_{\rm pl}$ by the bundle of rays destined for our telescope also decreases, thus probing less of the variance in the magnetic field direction and resulting in a higher polarized fraction.

Not surprisingly, if we neglect in the birefringence of magnetosphere, we sometimes find that smaller stars do exhibit smaller polarized fractions (as Pavlov & Zavlin 2000, found). This is most apparent for the case where the magnetic pole makes an angle of 60° with respect to the line of sight. If the magnetic pole makes a smaller angle with the line of sight, the trend of the polarization with the compactness is less apparent. Because the flux from the stellar surface is concentrated near the magnetic poles, only if the image contains both poles can there be a substantial reduction in the polarization. If one pole makes a 60°-angle with the line of sight, the other pole is visible for all three stellar radii that we have considered and as the stellar radius decreases more of the second polar region becomes visible, and the total polarization decreases. On the other hand, if the pole makes a 30°-angle with the line of sight, only if the stellar radius is less than 8.55 km are both poles visible. In this case, the trend with radius is more complicated. Regardless, because the vacuum birefringence strongly affects the observed polarization, understanding these trends in detail only provides a bridge to compare our results with earlier results with have neglected the QED effects.

3.2. Angular Dependence

Comparing the results depicted in the upper and lower panels of Fig. 2 explores the extent of polarization as a function of frequency and angle. The results here confirm the results of Heyl et al. (2003) (see their Fig. 5). The extent of the observed polarization increases with the angle between the line of sight and the dipole axis. This effect is apparent both with and without vacuum polarization in the magnetosphere. The source of this trend is quite straightforward. If the observer is looking straight down onto the magnetic pole of the star, the net polarization must vanish by symmetry, independent of vacuum birefringence. As this angle increases so to must the net polarization. Whether the net polarization attains a maximum before the angle reaches ninety degrees will depend on the details. If polarization-limiting radius is much larger than the stellar radius, the polarization will increase until the angle between the line of sight and the pole reaches ninety degrees. This is also the case if one neglects the gravitational defocussing of the stellar

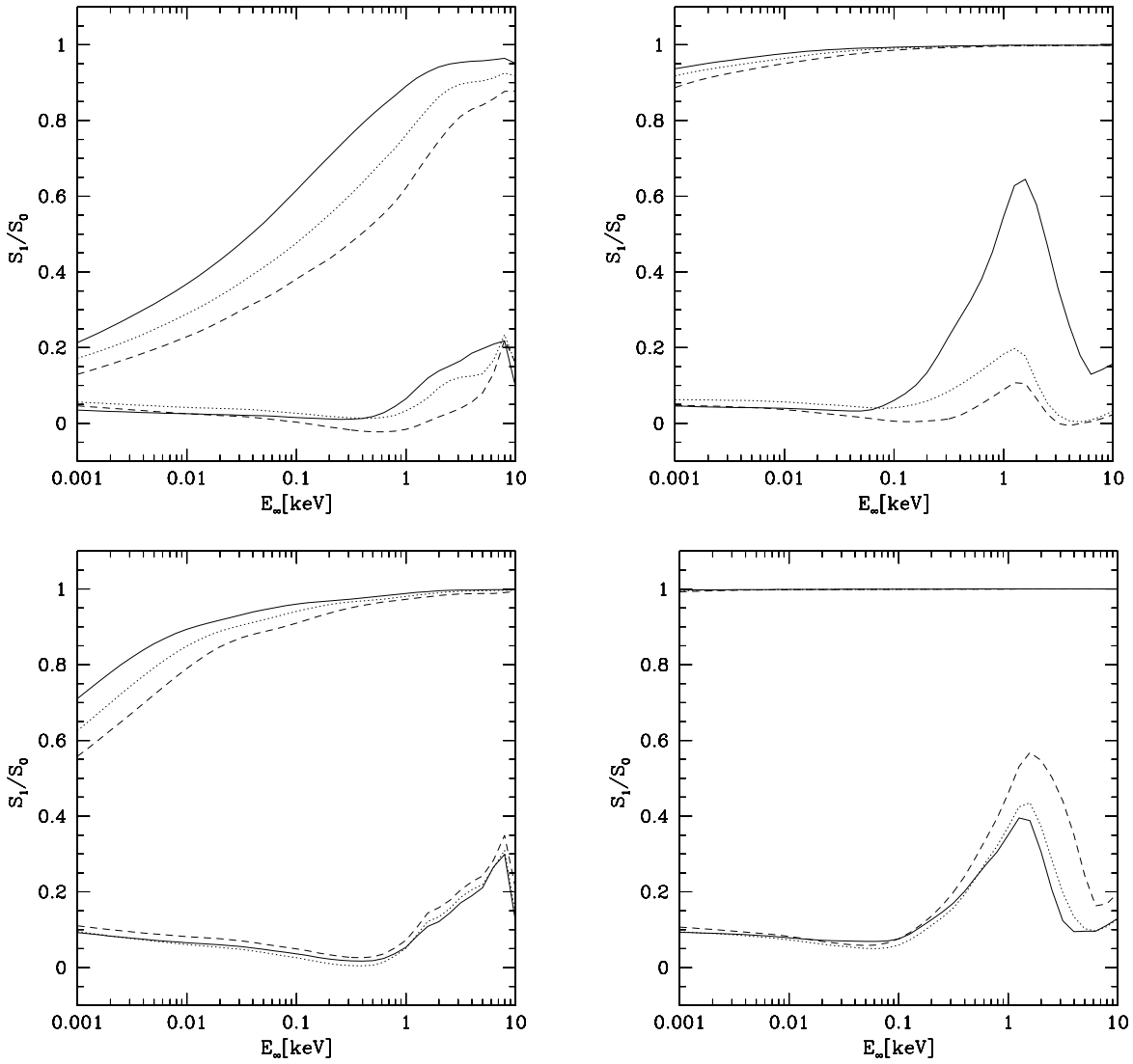

Fig. 2.— The extent of the polarization as a function of energy, angle and stellar radius. $S_1/S_0 = 1$ denotes light fully polarized perpendicular to the projection of the dipole into the sky. $S_1/S_0 = -1$ is light fully polarized parallel to this vector. In the upper panels, the magnetic pole makes an angle of 30° with the line of sight. In the lower panels the angle is 60°. The lower set of curves trace the results without vacuum polarization, and the results for the upper curves include it. The solid, dotted and dashed curves follow the result for 8, 10 and 12 km neutron stars. The mass of the star is 1.4 $M_\odot$. The effective temperature at the magnetic pole is $10^{6.5}$ K. The left panel is for a magnetic moment of $\mu = 10^{30}$ G cm^3 and the right panel is for $\mu = 10^{32}$ G cm^3.

surface, *i.e.* in the limit of $R \gg GM/c^2$. If $R \sim GM/c^2$ and the polarization-limiting radius is not much larger than R, the behavior may be more complicated.

3.3. Comparison with Earlier Results

These results presented here agree well with the trends explored in Heyl et al. (2003). Specifically, the polarization of the flux increases with the frequency of the radiation, with the angle between the magnetic dipole moment and the line of sight and with the strength of the magnetic dipole moment, and decreases as the radius of the star increases. All of these effects are driven by the QED-induced vacuum polarization in the magnetosphere. The most recent comparable work other than our own is that of Pavlov & Zavlin (2000). The study of Pavlov & Zavlin (2000) differs from ours in three important respects. First, Pavlov & Zavlin (2000) neglected the effects of vacuum polarization in the magnetosphere. Second, Pavlov & Zavlin (2000) did not account for the fact that the temperature across the surface of the neutron star varies. Third, Pavlov & Zavlin (2000) used the diffusion approximation in calculating their atmosphere models while we used a more accurate complete linearization treatment.

By shutting off the vacuum polarization and the variation of the temperature across the surface we can attempt to reproduce the results of Pavlov & Zavlin (2000). This is depicted in the left panel of Fig. 3. The lower two curves are the results of Pavlov & Zavlin (2000) at $T_{\rm eff} = 10^6$ K for the two smaller radii depicted in Fig. 2. The middle three curves follow the results neglecting vacuum polarization for an isothermal surface at the same effective temperature. The qualitative agreement is good but quantitative disagreements arise due to the differing treatment of radiative transfer. The upper three lines include vacuum polarization for these same parameters.

The right panel of Fig. 3 depicts models in which the surface temperature varies according to Eq. 1. In this case a small portion of the star contributes the bulk of the flux at high energies, so not surprisingly the extent of polarization is larger above a few hundred electron volts than in the model depicted in left panel. The extent of the polarization at low energies is somewhat lower reflecting differences in the detailed treatment of the atmosphere upon which the low-energy flux strongly depends.

4. Discussion

We have found that the treatment of the vacuum polarization of the magnetosphere surrounding a neutron star is crucial to determine the polarized emission from the surface accurately.

We have also shown the effect that real atmospheres have on the polarization. The net polarization observed in this case is somewhat reduced since a surface element will have a lower intrinsic polarization to begin with, such that even complete alignment will not result with 100%

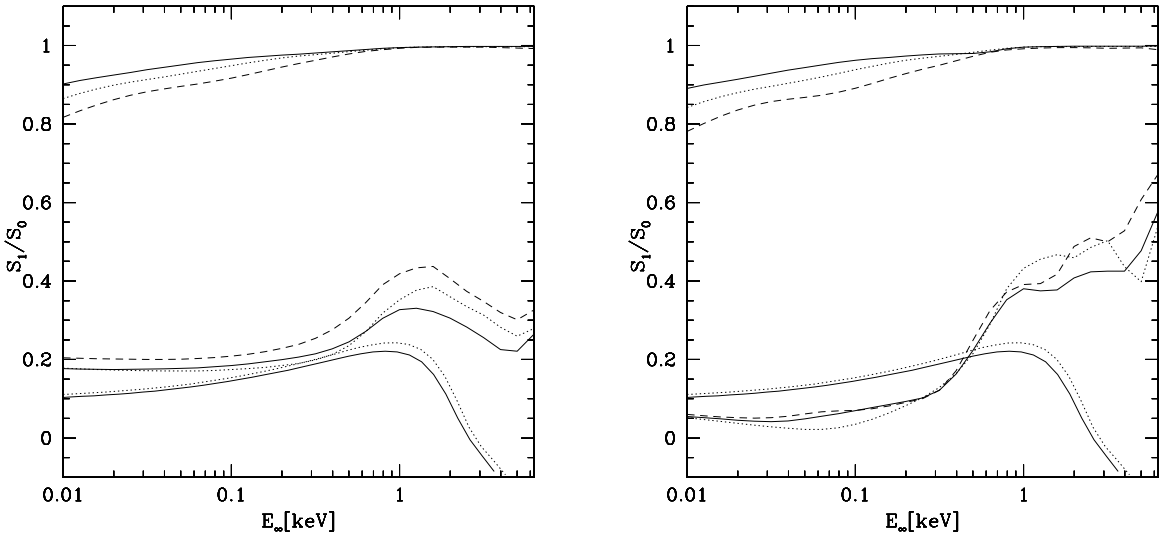

Fig. 3.— Comparison with the results of Pavlov & Zavlin (2000). The solid line, dotted and dashed curves trace results for 8, 10, and 12 km neutron stars with $M = 1.4\mathrm{M}_\odot$ and $\mu = 10^{30}$ G cm^3.. In both panels, the magnetic pole makes a 60° with the line of sight. The left panel assumes that the temperature of the star is constant over the surface as Pavlov & Zavlin (2000) did. The right panel accounts for the variable temperature of the surface. The uppermost curves include the radiative corrections of QED. The middle curves are our resutls without radiative corrections and the lowermost curves are the results obtained by Pavlov & Zavlin (2000).

polarization. Anomalous X-ray Pulsars (AXPs), if they are magnetars (neutron stars with surface magnetic fields of 10^{14} G or larger), should exhibit an extremely large polarization even at optical wavelengths. This could potentially be detected in the observed optical counterpart to an AXP, thus possibly verifying that AXPs are indeed magnetars.

In the optical/UV the polarized fraction depends quite strongly on μ and R. In Figure 2, the magnetic dipole moment varies by a factor of one hundred between the left and right panels. On each panel of curves, the radius varies between eight and twelve kilometers. Decreasing the stellar radius by a factor of 3/2 increases the observed polarized fraction by a factor of 1.3 to 1.7 for the more weakly magnetized stars, similar to that achieved by increasing the dipole moment by a factor of six, because the polarized fraction is approximately a function of $b_{\rm max}/r_{\rm pl}$. If the magnetic dipole moment of a neutron star is moderately constrained (*e.g.* by spin down), polarization observations can use this strong dependence to constrain the stellar radius.

Without the effects of QED alignment, the highest expected time-resolved polarized fraction is about 15%-25% under the most favorable conditions. However, the time-averaged measurement will typically be smaller. With the effects of QED alignment taken into account, the expected time-resolved polarization at X-rays is close to the maximum emitted by the atmosphere (50%-95%), with the time-averaged case being somewhat lower, but still larger on average than the highest time-resolved net polarization expected if QED is neglected. Under coincidentally unfavorable conditions, the time-averaged case can nevertheless be averaged to a low value. Namely, without time-resolved polarimetry one can prove, but not necessarily disprove the importance of QED polarization alignment. In such a case, it would be advantageous to look at the thermal emission of several NSs. If time-resolved polarimetry is available, then even one object could be used to verify the birefringence of the magnetized vacuum due to QED.

Support for this work was provided by the National Aeronautics and Space Administration through Chandra Postdoctoral Fellowship Award Number PF0-10015 issued by the Chandra X-ray Observatory Center, which is operated by the Smithsonian Astrophysical Observatory for and on behalf of NASA under contract NAS8-39073.

REFERENCES

Chang, P., Arras, P., & Bildsten, L. 2004, ApJ, 616, L147

Chang, P. & Bildsten, L. 2004, ApJ, 605, 830

Heyl, J. S. & Hernquist, L. 1998a, MNRAS, 300, 599

—. 1998b, MNRAS, 298, L17

—. 2001, MNRAS, 324, 292

Heyl, J. S. & Shaviv, N. J. 2002, Phys. Rev. D, 66, 023002

Heyl, J. S., Shaviv, N. J., & Lloyd, D. 2003, MNRAS, 342, 134

Ho, W. C. G., Lai, D., Potekhin, A. Y., & Chabrier, G. 2003, ApJ, 599, 1293

Lai, D. & Ho, W. C. 2003a, Physical Review Letters, 91, 071101

Lai, D. & Ho, W. C. G. 2003b, ApJ, 588, 962

Lloyd, D., Hernquist, L., & Heyl, J. S. 2003, ApJ, 593, 1024

Lloyd, D. A. 2003, MNRAS, submitted (astro-ph/0303561)

Mihalas, D. 1978, Stellar atmospheres (San Francisco, W. H. Freeman and Co., 1978. 650 p.)

Page, D. 1995, ApJ, 442, 273

Pavlov, G. G. & Zavlin, V. E. 2000, ApJ, 529, 1011

Perna, R., Heyl, J., & Hernquist, L. 2001a, ApJ, 553, 809

Perna, R., Heyl, J. S., Hernquist, L. E., Juett, A. M., & Chakrabarty, D. 2001b, ApJ, 557, 18

Shannon, R. M. & Heyl, J. S. 2004, Phys Rev Let, submitted

Özel, F. 2001, ApJ, 563, 276

—. 2003, ApJ, 583, 402

Turolla, R., Zane, S., & Drake, J. J. 2004, ApJ, 603, 265

Ventura, J. 1979, Phys. Rev. D, 19, 1684

Zane, S., Turolla, R., Stella, L., & Treves, A. 2001, ApJ, 560, 384

This preprint was prepared with the AAS LaTeX macros v5.2.